



# Topological Insight into Superabsorbent Hydrogel Network Structures: a $^1\text{H}$ Double-Quantum NMR Study

Xiaoai Guo,\* Solveig Theissen, Jan Claussen, Viet Hildebrand, Juliane Kamphus, Manfred Wilhelm, Burkhard Luy, and Gisela Guthausen\*

Superabsorbent polymer (SAP) hydrogels have pronounced water-absorbing and water-storing capacities, which are essential for numerous potential applications. It remains a challenge to better understand the network topology because of their amorphous and anisotropic structures. Synthesis parameters such as monomer concentration, degree of neutralization and crosslinking, and surface crosslinking are varied to correlate structural changes in the network with low-field proton double-quantum ( $^1\text{H}$  DQ) NMR results.  $^1\text{H}$  DQ-NMR data are processed by a reliable, user-independent analysis approach to determine the fractions of network defects, of mobile sol components, and of network chains as well as the residual dipolar coupling distribution in SAPs. In addition, results obtained by applying different distributions to describe the DQ buildup curves are quantified and compared. The correlation between topological and synthesis parameters as well as the impact of temperature, swelling, and solvent of SAP on DQ signals is investigated and discussed.

drug delivery, cosmetics, separation, and wastewater treatment, or serve as a versatile alignment medium for measurement of anisotropic parameters.<sup>[1–6]</sup> Hydrogels display both chemical and physical crosslinks, depending on the synthesis methods.<sup>[7,8]</sup> Compared to physical crosslinks, chemical covalent crosslinks are, mechanically and thermally, substantially more stable. Superabsorbent polymers (SAP) are made of lightly crosslinked hydrophilic polymer networks, and can absorb and retain extraordinarily large amounts of water or aqueous solution.<sup>[9,10]</sup> The degree of crosslinking has a direct impact on swelling and gel strength. Crudely speaking, an increase in the crosslinking density leads to a decrease in swelling capacity and to an increase in mechanical strength as measured via the gel strength. In addition, the probability

## 1. Introduction

Hydrogels are attracting significant attention due to their unique hydrophilic nature. They have vast potential applications in the fields of hygiene products, agriculture, biomedicine,

of chains to grow decreases at a lower monomer concentration, which leads to a larger concentration of extractables, e.g., oligomers, residual monomers, and non-crosslinked small polymer chains, as well as to more network defects such as dangling ends, loops, and crosslinker–crosslinker shortcuts.<sup>[11]</sup> The higher the initial monomer concentration, the larger the effective crosslinking density of the hydrogels and the smaller their swelling capacity due to different side reactions and close proximity during reaction.<sup>[12]</sup> Compared to ideal gels with a homogeneous crosslinking, real and industrial hydrogels always exhibit an inhomogeneous crosslinking, i.e., a density distribution, known as spatial gel inhomogeneity<sup>[13]</sup> along with additional topological network defects.<sup>[11,12]</sup> The extent of inhomogeneity depends on the polymerization mechanism and reaction temperature.<sup>[14–16]</sup> Besides the nanostructural heterogeneity, the network dilation and the release of topological constraints such as next-neighbor packing or entanglements during the swelling process lead to swelling inhomogeneity.<sup>[17]</sup> Loosely crosslinked networks swell more than densely crosslinked networks.<sup>[13]</sup>

Various analytical approaches have been applied to investigate the spatial inhomogeneity of polymer gels on length scales ranging from a few nanometers (typical mesh size) to hundreds of nanometers (typical length of spatial variation of the crosslinking density).<sup>[11]</sup> Due to the insufficient spatial resolution of a conventional optical microscope, high-/super-resolution optical microscopes have been used to directly measure inhomogeneous nanostructures of polymer networks;

Dr. X. Guo, Prof. M. Wilhelm  
Institute for Chemical Technology and Polymer Chemistry  
Karlsruhe Institute of Technology (KIT)  
Engesserstrasse 18, 76128 Karlsruhe, Germany  
E-mail: xiaoai.guo@kit.edu

S. Theissen, Prof. G. Guthausen  
Institute for Mechanical Process Engineering and Mechanics  
Karlsruhe Institute of Technology (KIT)  
Strasse am Forum 8, 76131 Karlsruhe, Germany  
E-mail: gisela.guthausen@kit.edu

Dr. J. Claussen, Dr. V. Hildebrand, Dr. J. Kamphus  
Procter & Gamble Service GmbH  
Sulzbacher Strasse 40, 65824 Schwalbach am Taunus, Germany

Prof. B. Luy  
Institute of Organic Chemistry and Institute for Biological Interfaces 4  
Karlsruhe Institute of Technology (KIT)  
Fritz-Haber-Weg 6, 76131 Karlsruhe, Germany

Prof. G. Guthausen  
Engler-Bunte-Institut  
Chair of Water Chemistry and Water Technology  
Karlsruhe Institute of Technology (KIT)  
Engler-Bunte-Ring 1, 76131 Karlsruhe, Germany

DOI: 10.1002/macp.201800100

e.g., nanometric inhomogeneity of poly(methyl methacrylate) networks was observed by fluorescence scanning near-field optical microscopy.<sup>[18]</sup> The size of short-chain domains in heterogeneous bimodal poly(dimethylsiloxane) networks was investigated by high-resolution confocal fluorescence microscopy.<sup>[19]</sup> Nanoscale in situ characterization of distinct polymeric subunits of poly(*N*-isopropylacrylamide) microgels was performed during swelling and collapse of individual particles using super-resolution optical reconstruction microscopy,<sup>[20]</sup> to name just a few. Transmission and scanning electron microscopes with higher spatial resolution or smaller voxel sizes are widely used to characterize nanostructural inhomogeneity in polymer networks, e.g., the inherent inhomogeneity of crosslinks on length scales from tens to hundreds of nanometers.<sup>[21,22]</sup> The structural inhomogeneity in a dry gel observed by electron microscopy is usually underestimated compared to that measured in a swollen gel.<sup>[11]</sup> The polymer gels require a special sample preparation procedure and restrictive measuring conditions such as drying or lyophilization. Drying may cause morphological changes. Freeze-fracture cryogenic electron microscopy (FF-Cryo-SEM or -TEM) can overcome vacuum-induced sample deformation.<sup>[23]</sup> Thus, noninvasive, fast, and reliable methods are searched for to characterize the polymeric network and its inhomogeneity. Since the inhomogeneity of polymer gels is closely related to spatial concentration fluctuations, it has been investigated with scattering methods such as light scattering,<sup>[15,24,25]</sup> small-angle X-ray and neutron scattering, or by a combination of both.<sup>[21,26–28]</sup> Several spectroscopy techniques such as nuclear magnetic resonance (NMR), ultraviolet–visible spectroscopy, Fourier transform infrared spectroscopy, and Raman spectroscopy have been utilized to study the molecular and phase evolution during formation of hydrogels.<sup>[29,30]</sup> Among them, especially proton double-quantum (<sup>1</sup>H DQ) NMR has become one of the most powerful and quantitative methods.<sup>[31–35]</sup> It addresses the <sup>1</sup>H–<sup>1</sup>H dipolar couplings, which depend on the orientation of chain segments, i.e., geometry, distance, and chain dynamics. The time-averaged <sup>1</sup>H dipolar coupling for isotopically mobile chains like defects and sol approaches zero on the typical time scales of the experiment, whereas a finite residual dipolar coupling (RDC) is observed in crosslinked polymer gels with anisotropic segmental motion.<sup>[31]</sup> A distribution of RDCs and the fraction of network defects were determined in <sup>1</sup>H DQ-NMR experiments.<sup>[32,33,36]</sup> Modeling and simulation of hydrogel structures help to understand their volume transition behavior. Models to be mentioned are thermodynamic models, transport models, multiphase mixture theory, and molecular simulations.<sup>[37]</sup> Experimentally, robust and cost-efficient static low-field <sup>1</sup>H DQ-NMR instruments are easy to handle and therefore are suitable for quality control of SAP hydrogels,<sup>[32,35]</sup> although solid-state magic-angle spinning recoupling <sup>1</sup>H DQ-NMR allows studying spectrally resolved RDCs.<sup>[38–41]</sup>

As stated above, SAP hydrogels show very large water-absorbing and water-storing capacities, which are closely associated with polymer network structures, charge density, and diffusion of fluidic guest molecules, such as water, synthetic solutions, or biological fluids and/or ions in fluids. Diffusion in polymer networks is complex and depends on concentration and swelling degree of the polymer gel.<sup>[42,43]</sup> Diffusion is related

to the kinetics of swelling, e.g., the absorption speed. The swelling capacity is also restricted by the degree of crosslinking of SAPs. Furthermore, Na<sup>+</sup> is present in the SAP due to the neutralization of carboxylate groups. Upon contact with water, the dissociated sodium carboxylate groups lead to an increase in osmotic pressure within the hydrogel and thus the swelling capacity.<sup>[44,45]</sup> To get a more comprehensive description of the topology in a SAP hydrogel and the dynamics of polymer networks, <sup>1</sup>H DQ-NMR was applied to investigate SAP hydrogels with different reaction parameters such as the degree of neutralization, the monomer concentration, and the degree of crosslinking, as well as the surface crosslinking. The RDC distribution and the fractions of network defects, mobile sol components, and network chains were measured by <sup>1</sup>H DQ, including the reference signal. To avoid or reduce the subjective error in the commonly applied stepwise DQ data analysis, a tri-exponential fit to the modified reference signal was performed to determine the structural parameters of swollen SAP. Finally, the RDC distributions were extracted from the data. Results are quantified and compared exploring different numerical approaches. The correlation between topology and synthesis parameters as well as the impact of temperature, swelling, and solvent on DQ-signals were investigated and discussed.

## 2. Experimental Section

### 2.1. Materials and Sample Preparation

The SAP hydrogels were synthesized by Procter & Gamble Service GmbH (Schwalbach, Germany) (Table 1). The SAP powders have particle sizes in a range of 150–710 μm. For <sup>1</sup>H DQ-NMR, the samples were prepared by repeatedly washing in deuterated water (D<sub>2</sub>O) and swelling. For a mass

**Table 1.** Properties of the superabsorbent polymer (SAP) hydrogels.

Hydrogel samples SAP DN AA DC	DN [mol%]	AA [wt%]	DC [mol%]
SAP 75 20 0.3	75	20	0.3
SAP 75 25 0.3	75	25	0.3
SAP 75 30 0.3	75	30	0.3
SAP 75 20 1	75	20	1.0
SAP 75 25 1	75	25	1.0
SAP 100 25 0.3	100	25	0.3
SAP 100 25 1	100	25	1.0
SAP 75 20 0.3 R <sup>a)</sup>	75	20	0.3
SAP 75 20 0.3 RSXL1 <sup>b)</sup>	75	20	0.3
SAP 75 20 0.3 RSXL2 <sup>b)</sup>	75	20	0.3

<sup>a)</sup>Synthesis with a different reactor type as compared to SAP 75|20|0.3. The sample was used as a reference for SXL SAP; <sup>b)</sup>Synthesis with a different reactor type, “surface crosslinked SAP (RSXL).”; DN: Degree of neutralization, defined as the mole ratio of NaOH to acrylic acid; AA: Solid content, i.e., monomer concentration *Q* at the beginning of polymerization, defined as the mass ratio of polymer synthesis educts to water content; DC: Degree of crosslinking, defined as the mole ratio of cross linker to acrylic acid.

ratio of SAP:D<sub>2</sub>O = 1:9, 35 mg of dry SAP was mixed with 315 mg of D<sub>2</sub>O (99.9% deuterated, Merck, Germany) in a 10 mm NMR glass tube (67 mg dry gels for 1:5). To avoid evaporation, the tubes were stoppered and sealed with parafilm and then left to swell and exchange ions for 24 h. The swollen samples were put in a vacuum drying oven (HER-AEUS, Hanau, Germany) at 70 °C and 100 mbar for 6 h to remove volatile substances. Gravimetric analysis indicated that the mass loss was lower than 1% compared to the original SAP. The washed and dried samples were mixed again with D<sub>2</sub>O at the same mass ratio and were swollen for more than 24 h before performing the <sup>1</sup>H DQ-NMR measurements. The filling level of the NMR glass tube was kept between 8 and 10 mm.

## 2.2. NMR Instrument and Measurements

The <sup>1</sup>H DQ-NMR experiments were performed on a low-field NMR spectrometer (Bruker “the minispec” mq20, Bruker, Germany) operating at a <sup>1</sup>H resonance frequency of 20 MHz ( $B_0 \approx 0.5$  T). The 10 mm NMR glass tube containing the prepared sample was placed inside the probe so that the sample was located in the center of the radio frequency coil to ensure relatively homogeneous  $B_0$  and  $B_1$  magnetic fields. The preset measuring temperature, e.g., at 39.5 or 55 °C, was controlled by a temperature controller (BVT, Bruker, Germany). Both <sup>1</sup>H DQ build-up signal  $S_{DQ}$  and reference signal  $S_{ref}$  were acquired (Table 2)<sup>[32,34]</sup> to determine the RDC distribution  $D_{res}$ , the fractions of network defects  $B$ , and mobile sol components  $C$ . Repeated measurements (5×) on the same swollen sample showed that an empirical relative standard deviation of the acquired raw data amounts to  $\approx 5\%$ . Thus, the repeatability of the spectrometer itself was good enough in the DQ experiments, implicating also that swollen hydrogels are physically and chemically stable within the measurement time. To check the sample uniformity and representativeness, the same dry hydrogel was used to prepare five independent samples. The relative empirical standard deviation of the acquired raw data was less than 6%, showing a sufficiently good reproducibility of sample preparation. Besides, DQ experiments applying different recycle delays (0.3 and 0.5 s) indicated that the use of the shorter recycle delay leads to only little variation in the determined structural parameters, but reduces the DQ overall measuring time significantly.

**Table 2.** Parameters of <sup>1</sup>H DQ-NMR.

Parameter	Value
Number of scans	512
Number of DQ build-up points	52
Recycle delay	0.3 and 0.5 s
90° pulse duration	4.5 $\mu$ s
180° pulse duration	8.9 $\mu$ s
Dead time	11 $\mu$ s
Measuring temperatures	39.5 and 55 °C

## 3. Results and Discussion

### 3.1. Fractions of Network Defects and Mobile Sol Components

In a low-field DQ-NMR experiment, the <sup>1</sup>H DQ build-up  $S_{DQ}$  and a reference decay  $S_{ref}$  are acquired (Figure 1).  $S_{DQ}$  depends on the evolution time  $\tau_{DQ}$  under a dipolar DQ average Hamiltonian, while  $S_{ref}$  comprises the total magnetization.<sup>[32,46]</sup> Conventionally, the raw data of DQ build-up and reference decay signals were normalized to  $S_{ref}(\tau_{DQ} \rightarrow 0)$  for further data processing in a stepwise fitting procedure.<sup>[32,34]</sup> The contribution from the mobile sol components  $C$  with small molecular weight and high mobility such as residual monomers and extractables (non-crosslinked small polymer chain, oligomer) is usually taken into account by an exponential decay  $C \cdot \exp(-c \cdot \tau_{DQ})$  for  $\tau_{DQ} > 30$  ms, where  $c$  is the relaxation rate of this mobile fraction (Figure 1a). In case of SAP 75|30|0.3 sample swollen at a mass ratio of SAP:D<sub>2</sub>O = 1:9,  $C = 4.27\%$  was determined by back extrapolation to  $\tau_{DQ} = 0$ . The time range of the fit was empirically chosen based on  $S_{DQ}$  as it becomes very noisy for  $\tau_{DQ} > 30$  ms. Thus, the DQ signal is assumed to be negligible

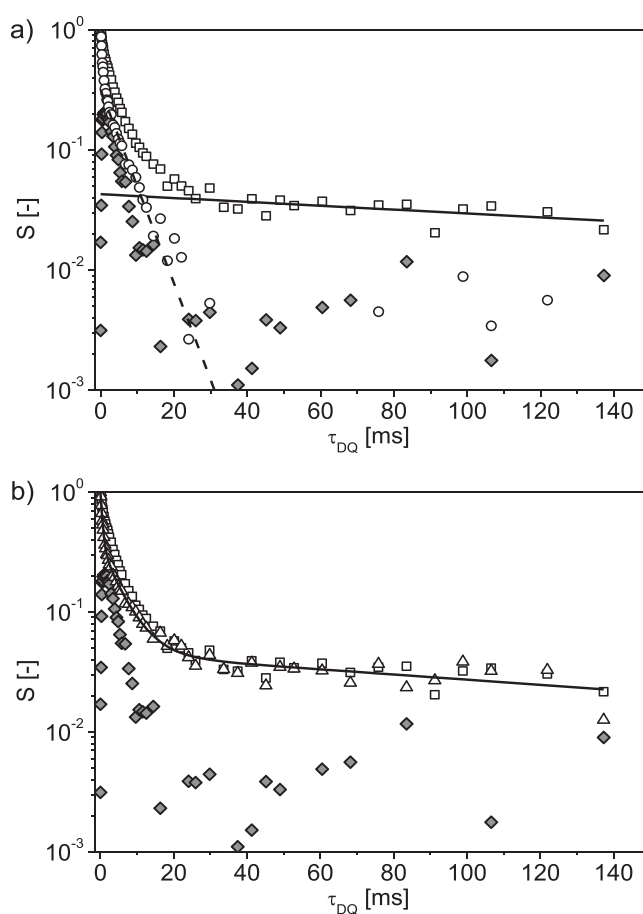


**Figure 1.** <sup>1</sup>H DQ build-up signal  $S_{DQ}$  (◆) and reference signal  $S_{ref}$  (□) exemplarily for the sample SAP75|30|0.3 in a semi-logarithmic plot. a) Fractions of network defects  $B$ , mobile sol components  $C$ , and gel network chains  $A_N$  determined by the common stepwise fitting [solid line fit to  $S_{ref}$ , dashed line fit to  $S_{DQ}$  (○)]. b) Analysis of  $S_{ref} - S_{DQ}$  data (△) with the model in Equation (1) (solid line).

in that long time range. The reduced signal intensity  $S_{\text{red}} = S_{\text{ref}} - S_{\text{DQ}} - C \cdot \exp(-c \cdot \tau_{\text{DQ}})$  reflects the fraction of network defects like dangling chains and loops amongst others. This fraction  $B$  is obtained by fitting another exponential decay  $B \cdot \exp(-b \cdot \tau_{\text{DQ}})$  (dashed line in Figure 1a). The intermediate fitting range was chosen empirically in the linear range of  $S_{\text{red}}$  in the semilogarithmic plot from  $\tau_{\text{DQ}}$  near the maximum of  $S_{\text{DQ,max}}$  to the start fitting time point ( $\tau_{\text{DQ}} \approx 30$  ms) of  $S_{\text{ref}}$ . The fraction of network defects is  $B = 31.40\%$  in SAP 75|30|0.3. Thus, the fraction of hydrogel network chains  $A_N$  remains as  $A_N = 1 - B - C = 64.33\%$  for the given sample. In this model, the SAP hydrogel signal can be roughly attributed to three fractions: the network chains  $A_N$ , the defects  $B$ , and the mobile fraction  $C$ .

In the stepwise fitting procedure, two time ranges have to be manually defined (Figure 1a).  $\tau_{\text{DQ}}$  of  $S_{\text{DQ,max}}$  depends on the SAP. It does not appear to be easy to define these fitting ranges due to the signal-to-noise ratio (S/N) in the low-field DQ experiments and different DQ build-up response times. Subjective errors are inevitable, and automation is impossible when aiming for quality control. To illustrate this effect,  $C$  and  $B$  were determined choosing different fitting ranges (Table 3). The variation of  $S_{\text{ref}}$  fitting range from [20.17, 137.29] to [52.81, 137.29] ms leads to about 7.9% relative deviation of  $C$  and 0.7% of  $B$ . Changing the  $S_{\text{red}}$  fitting range near the maximum of  $S_{\text{DQ,max}}$  results in a significant deviation in  $B$  of about 24%. The proper choice and definition of the two fitting ranges are therefore essential for a correct data interpretation.

To reduce the potential error in data analysis,  $S_{\text{ref}} - S_{\text{DQ}}$  was explored for calculation of  $B$ ,  $C$ , and  $A_N$ . This signal difference only considers single-quantum coherences that do not result from relaxation effects of DQ transitions (neglecting multi-quantum coherences).  $S_{\text{ref}} - S_{\text{DQ}}$  mostly delivers signal from uncoupled mobile components and network defects. In a first approximation  $S_{\text{ref}} - S_{\text{DQ}}$  can be modeled by a tri-exponential function

**Table 3.** Fractions of network defects  $B$  and mobile components  $C$  depend on the fitting ranges in the common stepwise fitting procedure.

$S_{\text{ref}}$ fitting range [ms]	Fraction of mobile components $C$ [%]	$S_{\text{red}}$ fitting range [ms]	Fraction of network defects $B$ [%]
20.17–137.29	5.01	2.41–29.77	31.90
25.93–137.29	4.28		31.41
29.77–137.29	4.27		31.40
33.61–137.29	3.90		31.15
37.45–137.29	4.00		31.22
41.29–137.29	4.18		31.34
45.13–137.29	4.02		31.23
48.97–137.29	4.53		31.61
52.81–137.29	4.41		31.51
29.77–137.29	4.27	2.41–29.77	31.40
		2.17–29.77	32.73
		1.93–29.77	34.62
		1.69–29.77	35.48
		1.45–29.77	37.21
		1.21–29.77	38.95

$$S_{\text{ref}} - S_{\text{DQ}} = A \cdot \exp(-a \cdot \tau_{\text{DQ}}) + B \cdot \exp(-b \cdot \tau_{\text{DQ}}) + C \cdot \exp(-c \cdot \tau_{\text{DQ}}) \quad (1)$$

where  $C$  corresponds to the fraction of mobile sol components in the long time range, and  $B$  represents the fraction of network defects. As  $\tau_{\text{DQ}}$  approaches zero,  $S_{\text{ref}} - S_{\text{DQ}} = 1$ , i.e.,  $A + B + C = 1$ . The numerical fit parameter  $A$  in Equation (1) is therefore related to  $A_N$ . However, as DQ coherences are neglected, the amplitude  $A$  does not necessarily deliver the actual fraction of crosslinked polymer chains  $A_N$  in the SAP hydrogel. Variables  $b$  and  $c$  in Equation (1) represent again the relaxation rates of the fractions  $B$  and  $C$ , respectively. The fraction of network defects such as dangling chains and loops relaxes faster than the fraction of mobile sol components ( $b \gg c$ ), which agrees well with the experimental results ( $b = 184 \text{ s}^{-1}$ ,  $c = 5 \text{ s}^{-1}$ ). This model describes the data well (Figure 1b), resulting in the fractions of network defects ( $B = 30.6\%$ ) and mobile sol components ( $C = 4.5\%$ ). Thus, the fraction of hydrogel network chains  $A_N$  amounts to 64.9% within this model. To compare the fit quality of both models, the adjusted  $R^2$  has been used. In the stepwise fitting procedure, the fit results of the fractions of network defects  $B$  and mobile sol components  $C$  have the adjusted  $R^2$  values of 0.9891 and 0.3051, respectively. The small adjusted  $R^2$  value is due to the signal-to-noise ratio in the long time range. Using Equation (1), the adjusted  $R^2$  amounts to 0.9972. The new approach shows a significantly improved statistic, leading to a more reliable method. Experiments on other SAP hydrogels in the current study confirmed that the tri-exponential fit describes the data of  $S_{\text{ref}} - S_{\text{DQ}}$  very well and reliably, resulting in the structural parameters  $B$ ,  $C$ , and  $A_N$  (Table 4). To summarize, as compared to the stepwise fitting procedure with a need for manual choice of two different fitting ranges, the proposed user-independent fit model has the advantage of a better numerical stability in the DQ-NMR data analysis, largely reducing the subjective error and opens up the possibility for automation of data analysis with respect to quality control application of the low-field DQ-NMR.

### 3.2. Residual Dipolar Coupling Distribution

To determine the RDC distribution in hydrogel networks, the DQ build-up signals are further normalized to the sum of  $S_{\text{DQ}}$  and  $S_{\text{ref}}$  after subtraction of the contributions of uncoupled mobile sol components and network defects. Incoherent relaxation effects can thus be removed. The resulting  $S_{\text{nDQ}}$  depends on the RDC distribution related to the gel network and reaches a plateau value of 0.5 in the long time limit (Figure 2a, Equation (2)). The shape of the RDC distribution  $P(D_{\text{res}})$  was assumed to be Gaussian with a mean  $D_{\text{res,mean}}$  and a width  $\sigma$  in a first approach<sup>[32,33]</sup>

$$S_{\text{nDQ}}(\tau_{\text{DQ}}) = 0.5 \left[ 1 - \frac{\exp\left(-\frac{0.4 D_{\text{res,mean}}^2 \tau_{\text{DQ}}^2}{1 + 0.8 \sigma^2 \tau_{\text{DQ}}^2}\right)}{\sqrt{1 + 0.8 \sigma^2 \tau_{\text{DQ}}^2}} \right] \quad (2)$$

**Table 4.**  $^1\text{H}$  DQ-NMR results of  $A_N$ ,  $B$ ,  $C$ ,  $D_{\text{res,mean}}$ ,  $\sigma$ , and  $r = \sigma/D_{\text{res,mean}}$  for different swollen SAP hydrogel samples ( $m_{\text{SAP}} : m_{\text{D}_2\text{O}} = 1 : 9$ ).

Sample	Fractions <sup>a)</sup>			Gaussian (fit) <sup>b)</sup>			A-I function kernel (reg.) <sup>c)</sup>			Gaussian kernel (reg.) <sup>c)</sup>		
	$A_N$ [%]	$B$ [%]	$C$ [%]	$D_{\text{res,mean}}$ [kHz]	$\sigma$ [kHz]	$r$ [-]	$D_{\text{res,mean}}$ [kHz]	$\sigma$ [kHz]	$r$ [-]	$D_{\text{res,mean}}$ [kHz]	$\sigma$ [kHz]	$r$ [-]
SAP 75 20 0.3	51.56	42.88	5.57	1.99	1.24	0.63	2.11	1.55	0.73	2.14	1.39	0.65
SAP 75 25 0.3	56.81	37.32	5.87	2.08	1.30	0.63	2.31	1.77	0.77	2.34	1.72	0.74
SAP 75 30 0.3	64.90	30.60	4.50	3.19	1.87	0.59	3.37	2.39	0.71	3.47	2.32	0.67
SAP 75 20 1	56.44	35.77	7.79	3.80	2.29	0.60	3.83	2.64	0.69	4.08	2.83	0.69
SAP 75 25 1	64.81	29.25	5.94	4.82	2.71	0.56	4.90	3.20	0.65	5.28	3.58	0.68
SAP 100 25 0.3	54.52	38.75	6.72	5.25	3.35	0.64	5.45	4.72	0.87	5.65	5.22	0.92
SAP 100 25 1	58.90	33.96	7.14	7.75	4.83	0.62	6.61	7.54	1.14	6.47	8.17	1.26
SAP 75 20 0.3 R	56.81	38.71	4.48	1.25	1.03	0.82	1.36	1.02	0.75	1.47	1.14	0.78
SAP 75 20 0.3 RSXL1	57.91	35.24	6.85	2.36	1.77	0.75	2.56	2.24	0.88	2.68	2.26	0.84
SAP 75 20 0.3 RSXL2	54.47	35.57	9.96	2.49	1.76	0.70	3.44	3.78	1.10	3.67	4.40	1.20

<sup>a)</sup>Analysis with the model given by Equation (1); <sup>b)</sup>Gaussian-distributed fitting with Equation (2); <sup>c)</sup>Regularization procedure with Gaussian and A-I kernel functions, Equations (3)–(5).

$S_{\text{nDQ}}(\tau_{\text{DQ}})$  is nearly identical within the experimental error for  $\tau_{\text{DQ}} < 10$  ms (Figure 2a) when using the two above described approaches. At larger  $\tau_{\text{DQ}}$ , the noise in  $S_{\text{nDQ}}$  is significant. Equation (2) describes the  $S_{\text{nDQ}}$  data and reaches the expected plateau value of 0.5 at larger  $\tau_{\text{DQ}}$ . Both  $S_{\text{nDQ}}$  data lead to similar RDC distributions ( $D_{\text{res,mean}} = 3.22$  kHz and  $\sigma = 1.84$  kHz for stepwise procedure, and  $D_{\text{res,mean}} = 3.19$  kHz and  $\sigma = 1.87$  kHz for tri-exponential model).

Due to swelling and spatial variation of crosslinking, polymeric networks exhibit a chain length and crosslinking distribution. The “real” RDC distribution may deviate from the assumed Gaussian distribution. Alternative procedures such as numerical iterative regularization may result in suitable estimations.<sup>[33,47,48]</sup> The measured data  $S_{\text{nDQ}}$  can be expressed in the form of a Fredholm integral with the RDC distribution  $P(D_{\text{res}})$

$$S_{\text{nDQ}}(\tau_{\text{DQ}}) = \int_0^{\infty} K(D_{\text{res}}, \tau_{\text{DQ}}) \cdot P(D_{\text{res}}) \cdot dD_{\text{res}} \quad (3)$$

where  $K(D_{\text{res}}, \tau_{\text{DQ}})$  is the kernel function. A modified fast Tikhonov regularization algorithm was applied with user-defined kernel functions, e.g., a modified “Aragam-like” (A-I) function<sup>[33]</sup>

$$K(D_{\text{res}}, \tau_{\text{DQ}}) = 0.5 \left\{ 1 - \exp \left[ - (0.378 D_{\text{res}} \tau_{\text{DQ}})^{1.5} \right] \cdot \cos(0.583 D_{\text{res}} \tau_{\text{DQ}}) \right\} \quad (4)$$

or a Gaussian kernel function<sup>[32,49]</sup>

$$K(D_{\text{res}}, \tau_{\text{DQ}}) = 0.5 \left[ 1 - \exp \left( -0.4 D_{\text{res}}^2 \tau_{\text{DQ}}^2 \right) \right] \quad (5)$$

The regularization using these kernel functions results in RDC distributions (Figure 2b). The shapes of the distribution curves (Figure 2b) can be attributed to the inhomogeneous hydrogel network structure itself and/or to the swelling inhomogeneity if not to numerical instabilities due to the relatively high noise in the DQ data. The parameter  $\chi^2$ , which is the mean square deviation between fit and experimental data, increases fast for both Gaussian and A-I kernels with increasing

noise term  $\varepsilon$  above a critical value. Below this critical value of  $\varepsilon$  ( $\varepsilon_c \approx 0.006$  in Figure 2c), the parameters  $\chi^2$ ,  $D_{\text{res,mean}}$ , and  $\sigma$  change only slightly. The DQ build-up curve calculated via inversion using the Gaussian kernel describes the data well up to  $S_{\text{nDQ}} \approx 0.45$  (Figure 2a), covering  $\approx 90\%$  of the DQ build-up signal, while the build-up curve calculated with the A-I function kernel describes the data well in the whole range as does the Gaussian fit. It should be noted, however, that the RDC distribution reaching 0 at  $D_{\text{res}} = 0$  Hz coupling is physically not correct, which limits the significance of this kernel. Similar findings are summarized in literature.<sup>[33,36,39,50,51]</sup> Most recently, Naumova et al. have applied an empirical single-orientation A-I kernel function to study the anisotropically mobile protonated molecular segments.<sup>[52]</sup>

In summary, the  $S_{\text{nDQ}}$  data obtained with the proposed user-independent tri-exponential model and the conventional stepwise fit procedure through careful choice of two fitting ranges are nearly identical within the experimental error. Furthermore, direct Gaussian fit to the experimental data leads to an RDC distribution with a mean  $D_{\text{res,mean}}$  and a width  $\sigma$ , whereas numerical iterative regularization procedures using Gaussian and A-I function kernels without a predefined RDC shape result in suitable estimations of the real RDC distributions. The difference between the results,  $D_{\text{res,mean}}$  and  $\sigma$ , retrieved by regularization with two different kernel functions is small, and both are comparable to those obtained with direct Gaussian fit.

### 3.3. Correlation between DQ-NMR Results and Synthesis Parameters

The properties of SAP hydrogels are closely related to network structures which are determined by synthesis parameters. In this section, correlations between  $^1\text{H}$  DQ-NMR parameters ( $A_N$ ,  $B$ ,  $C$ ,  $S_{\text{nDQ}}$ , and  $D_{\text{res,mean}}$ ) and different reaction parameters (DN: degree of neutralization, AA: solid content, i.e., monomer concentration, and DC: degree of crosslinking) as well as surface crosslinking (SXL) are discussed.

### 3.3.1. Structural Parameters $A_N$ , $B$ , $C$ versus Synthesis Parameters (DN|AA|DC)

The comparison (Figure 3) shows that the fraction of network chains  $A_N$  increases with both AA and DC. As  $A_N$  and  $B$  are mutually dependent,  $B$  has to be considered as well. An increase of AA during synthesis results in larger amounts of chains while the distance between the chains decreases. In total, the fraction of crosslinked polymer rises. This increase amounts to  $\approx 5\%$ , for instance, from SAP 75|20|0.3 to 75|25|0.3 and up to 75|30|0.3. As the chain density is smaller in SAP of lower AA,  $B$  of those hydrogels is significantly larger. Increasing DC at constant AA causes an increase of the crosslinked fraction or an increased amount of the chemical crosslinks (cf. SAP 75|20|0.3 vs 75|20|1, SAP 75|25|0.3 vs 75|25|1, and SAP 100|25|0.3 vs 100|25|1). As a result of increasing DC,  $B$  is reduced by about 6%. Accordingly, the network fraction increases by 6%. Part of the defects is therefore crosslinked to the network fraction. In contrast, increasing the degree of neutralization DN during synthesis causes a decrease of  $A_N$ ; vice versa,  $B$  increases (cf. SAP 75|25|0.3 vs 100|25|0.3, and SAP 75|25|1 vs 100|25|1). For both parameters,  $A_N$  and  $B$ , the differences amount to about 6%.  $C$  increases slightly with increasing DN and decreasing AA. However, the change of  $C$  with DC is very small.

### 3.3.2. $S_{nDQ}$ and $D_{res}$ versus Synthesis Parameters (DN|AA|DC)

Normalized DQ build-up curves (Figure 4a) increase faster and more steeply with  $\tau_{DQ}$  upon increasing DC at constant AA and DN (cf. SAP75|20|0.3 vs SAP75|20|1, SAP75|25|0.3 vs SAP75|25|1, and SAP100|25|0.3 vs SAP100|25|1). In addition, an increase in AA leads to a faster and increasingly steeper DQ build-up as a function of  $\tau_{DQ}$  for constant DN and DC. This suggests that a higher monomer concentration increases the probability of the reaction, which results in less extractables and also less fraction of network defects, but a larger fraction of network chains (Figure 3). Larger polymer chains lead to more physical crosslinks such as entanglements. Faster DQ build-up corresponds to a higher level of dipolar couplings and a more constrained network. It is obvious that the RDC distribution (Figure 4b) shifts to larger  $D_{res,mean}$  and  $\sigma$  with increasing DC and AA, respectively (Table 4). An increase in chemical and/or physical crosslink density obviously results in larger  $D_{res,mean}$ . During the synthesis, a higher crosslinker concentration reduces the polymer mesh size and the mobility of polymer chains, giving rise to possibly inhomogeneous local structures and thus a broader RDC distribution. The inhomogeneity of hydrogels can also occur during swelling. By comparing DQ build-up curves of hydrogels with the same AA and DC but different DN (Figure 4a), the samples with DN = 100 mol% exhibit faster DQ build-up than those with DN = 75 mol% (cf. SAP75|25|0.3 vs SAP100|25|0.3 and SAP75|25|1 vs SAP100|25|1).  $D_{res,mean}$  values for the samples with a higher DN are larger than those with a lower DN (Figure 4c), and their RDC distributions are broader (Figure 4b). A good linear relationship between  $D_{res,mean}$  and  $\sigma$  has been found for the investigated SAPs (Figure 4d), i.e.,  $\sigma = 0.61D_{res,mean}$ . An increase in DN thus causes a more tightly crosslinked but

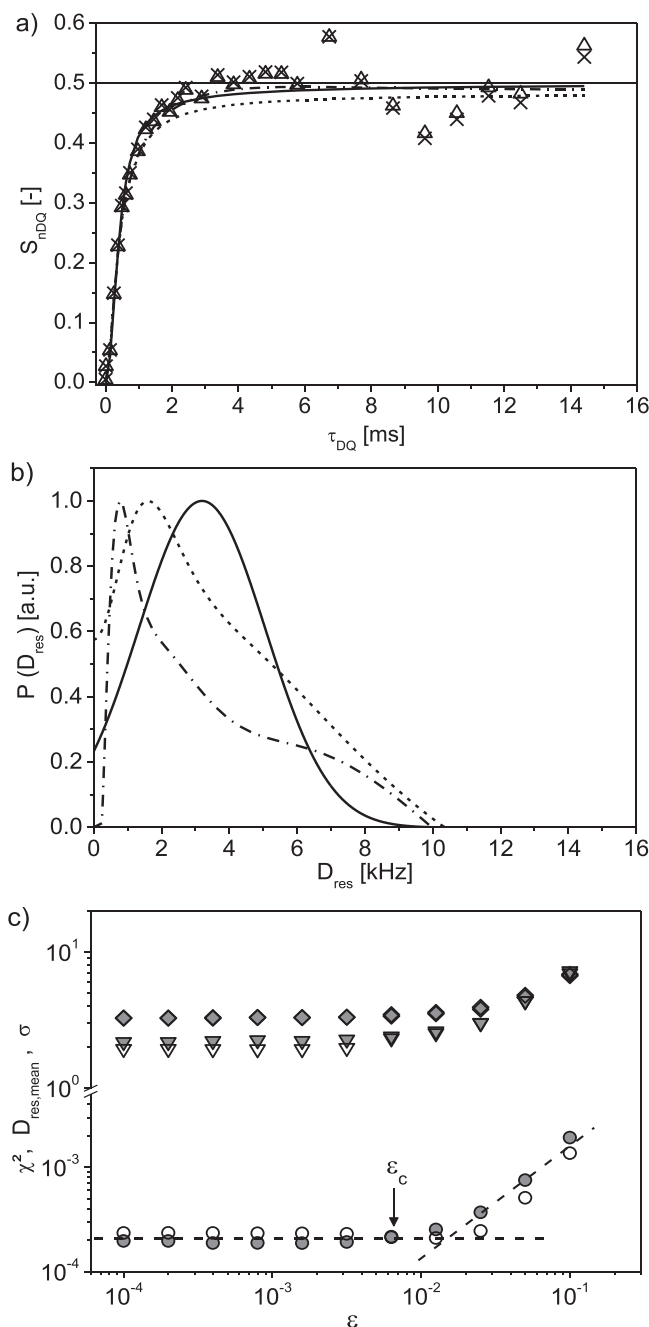


**Figure 2.** DQ-NMR on the example of the hydrogel SAP75|30|0.3. a) Normalized experimental  $^1\text{H}$  DQ build-up curves according to the common stepwise procedure ( $\times$ ), and tri-exponential model ( $\Delta$ ) and theoretical DQ build-up curves obtained by Gaussian fit (solid line) and by regularization with Gaussian (---) and A-I function (---) kernels. b) RDC distributions obtained by a fit to the experimental data ( $\Delta$ ) with Equation (2) (solid line) and by regularization with Gaussian (---,  $D_{res,mean} = 3.47$  kHz and  $\sigma = 2.32$  kHz) and A-I kernels (---,  $D_{res,mean} = 3.37$  kHz and  $\sigma = 2.39$  kHz). c)  $\chi^2$  ( $\bullet$ ),  $D_{res,mean}$  ( $\blacklozenge$ ), and  $\sigma$  ( $\blacktriangledown$ ) changing with error parameter  $\epsilon$  in the regularization procedure with A-I kernel (hollow dots correspond to Gaussian kernel).

inhomogeneous network structure. The protonated carboxyl groups on the hydrogel chains are able to form an intra- or interchain hydrogen bond like a temporal crosslinking. After

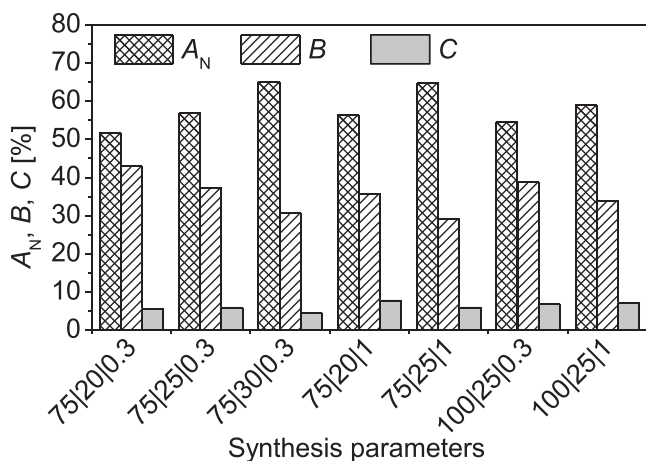


**Figure 3.** Structural parameters  $A_N$ ,  $B$ , and  $C$  determined by  $^1\text{H}$  DQ-NMR are shown for SAP hydrogels with different synthesis parameters (DN, AA, and DC).

swelling, however, the hydrogels undergo conformational changes because of electrostatic repulsion between negative charges (carboxyl groups) on the polymer, and the chains tend to expand. Oppositely charged counterions may be strongly attracted by the charged polymer chain due to a high charge density on the polymer chain, and the chain stiffness increases with ionization.<sup>[53]</sup> At a higher DN, more dissociated sodium carboxylate groups increase the osmotic pressure and thus the swelling capacity of the gel, although some free sodium ions may condense on the polymer chains in the swollen gel. If the level of crosslinker is fixed, the swelling capacity increases

with DN.<sup>[45]</sup> This may cause a larger inhomogeneity at higher DN, reflected by a broad RDC distribution. **Table 5** qualitatively summarized the influence of hydrogel synthesis parameters (DC, AA, and DN) on the characteristic parameters ( $D_{\text{res,mean}}$ ,  $\sigma$ ,  $A_N$ , and  $B$ ) determined by low-field  $^1\text{H}$  DQ-NMR.

### 3.3.3. DQ-NMR of SAP without and with Surface Crosslinking

In practical applications, SAP hydrogels are expected to exhibit high swelling capacity, which can be achieved usually by decreasing the crosslinking density. However, increasing the capacity would lead to a reduced liquid uptake at a higher pressure due to lower elasticity.<sup>[45]</sup> One way to improve the absorption at higher pressure and simultaneously avoid gel blocking is to utilize the low-crosslinked superabsorbent particles with a high crosslinking density at the particle surface, i.e., “core-shell” particles. The higher crosslinked shell can create tangential force, and such a “balloon effect” makes the SAP particles maintain the shape during swelling, improving their permeability and swelling capacity. A slightly crosslinked reference polymer hydrogel (DC = 0.3 mol%) was synthesized without surface crosslinking. Surface crosslinking was achieved by applying a crosslinking solution to the gel particles followed by a curing procedure.<sup>[45,54]</sup> Both the reference SAP hydrogel (SAP75|20|0.3|R) and the gels with surface crosslinking (SAP75|20|0.3|RSXL) were investigated by  $^1\text{H}$  DQ-NMR (**Figure 5**).

As expected, the fractions of network chains  $A_N$  and defects  $B$  did not vary for the SAP gel particles with and without surface crosslinking because of the same core crosslinking density. The

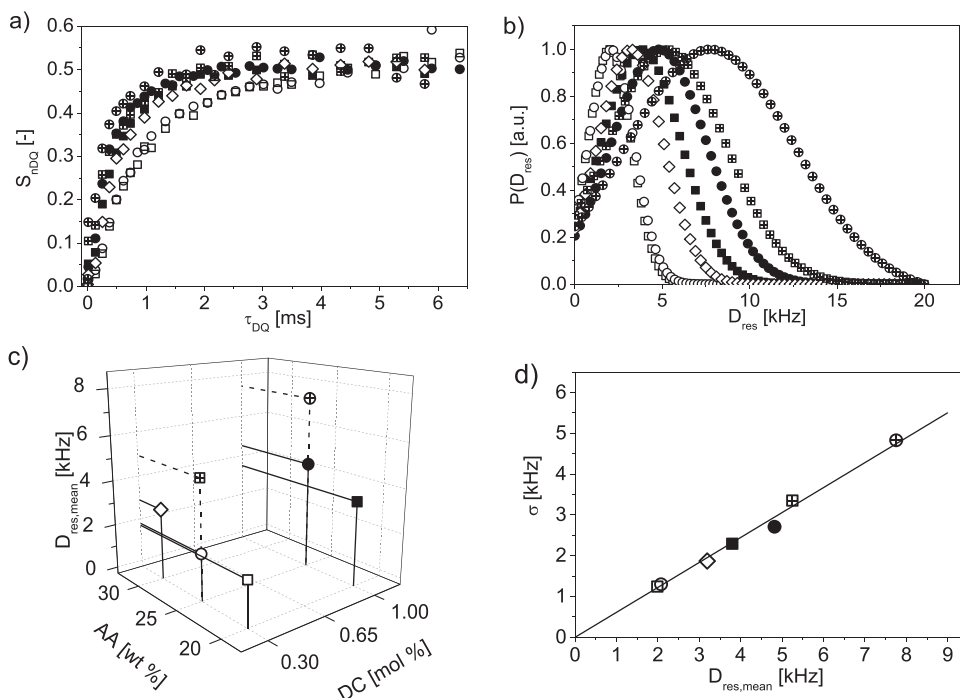


**Figure 4.**  $^1\text{H}$  DQ results for diverse SAP samples ( $\square$ , 75|20|0.3;  $\circ$ , 75|25|0.3;  $\diamond$ , 75|30|0.3;  $\blacksquare$ , 75|20|1;  $\bullet$ , 75|25|1;  $\boxplus$ , 100|25|0.3;  $\oplus$ , 100|25|1). a) Normalized DQ build-up curves. b) RDC distributions obtained by a Gaussian fit. c) Mean RDC  $D_{\text{res,mean}}$  for the variety of SAP. d) Relationship between mean RDC  $D_{\text{res,mean}}$  and distribution width  $\sigma$ .

**Table 5.** Qualitative correlation of synthesis parameters (DC, AA, and DN) and DQ-NMR parameters ( $D_{\text{res,mean}}$ ,  $\sigma$ ,  $A_N$ , and  $B$ ).

Increasing the parameters	Increase ( $\uparrow$ ) or decrease ( $\downarrow$ )			
	Mean RDC $D_{\text{res,mean}}$	Distribution width $\sigma$	Polymer chains $A_N$	Network defects $B$
Degree of crosslinking (DC)	$\uparrow$	$\uparrow$	$\uparrow$	$\downarrow$
Solid content (AA)	$\uparrow$	$\uparrow$	$\uparrow$	$\downarrow$
Degree of neutralization (DN)	$\uparrow$	$\uparrow$	$\downarrow$	$\uparrow$

surface crosslinking is formed only on the outmost layer of the SAP particles. The core network in the surface-crosslinked particles is almost not influenced by the surface crosslinking, which is consistent with the parameters determined by  $^1\text{H}$  DQ-NMR (Figure 5a). A high crosslinking density leads to a larger RDC. Thus, the RDC of RSXL is expected to be larger than that of the reference  $R$ . Regions with a high crosslinking density show larger RDCs than those with a low crosslinking density. The reference sample (SAP75|20|0.3|R) can be described by a monomodal distribution with  $D_{\text{res,mean}} = 1.25$  kHz and a relatively homogeneous mesh size distribution. A relatively uniform gel structure during the swelling leads to a relatively narrow RDC distribution. However, for SAP samples with surface crosslinking, the swelling capacity is lower compared to the reference SAP although they have the same core crosslink density.

For SAP samples with the two types of crosslinking (surface and core), the RDC distributions tend to be broader or even bimodal. Due to the surface crosslinking, the normalized DQ

build-up signals increase faster than that of the reference SAP (Figure 5b). Among three RDC distributions retrieved by regularization (Figure 5c), it is found that the maximum values are nearly identical because of the same core crosslinking. Both RSXL samples with surface crosslinking exhibit long-tail or bimodal distributions, statistically indicating that the portion of the higher crosslink density is smaller than that of the core. The contribution of surface crosslinking shows up in the RDC distribution nicely.

The bimodal distribution has been explored to describe the normalized DQ build-up signals for “core-shell” crosslinked hydrogel particles. A fit of the two-component superposition of Equation (2) to the  $S_{\text{inDQ}}$  data for SAP75|20|0.3|RSXL1 led to a bimodal RDC distribution ( $D_{\text{res1,mean}} = 0.94$  kHz,  $\sigma_1 = 0.38$  kHz; and  $D_{\text{res2,mean}} = 5.24$  kHz,  $\sigma_2 = 1.70$  kHz) (Figure 5d). The mode ( $D_{\text{res1,mean}}$ ,  $\sigma_1$ ) is related to the core, while the mode ( $D_{\text{res2,mean}}$ ,  $\sigma_2$ ) is related to the particle surface. A similar bimodal RDC distribution has been obtained for the other sample SAP75|20|0.3|RSXL2 ( $D_{\text{res1,mean}} = 1.02$  kHz,  $\sigma_1 = 0.37$  kHz and  $D_{\text{res2,mean}} = 6.19$  kHz,  $\sigma_2 = 1.71$  kHz) (cf. dashed line in Figure 5d). These results are very close to those obtained by regularization (Figure 5c). Slight difference between the values of mode ( $D_{\text{res2,mean}}$ ,  $\sigma_2$ ) for both RSXL samples can be attributed to the slight variation of the crosslinking density on the particle surface in the coating process.

Table 4 summarizes the  $^1\text{H}$  DQ-NMR results of  $A_N$ ,  $B$ ,  $C$ ,  $D_{\text{res,mean}}$ ,  $\sigma$ , and the relative distribution width  $r = \sigma/D_{\text{res,mean}}$  for different swollen SAP hydrogel samples ( $m_{\text{SAP}} : m_{\text{D}_2\text{O}} = 1 : 9$ ). The three different methods deliver comparable RDC distributions, while the difference between the results retrieved by

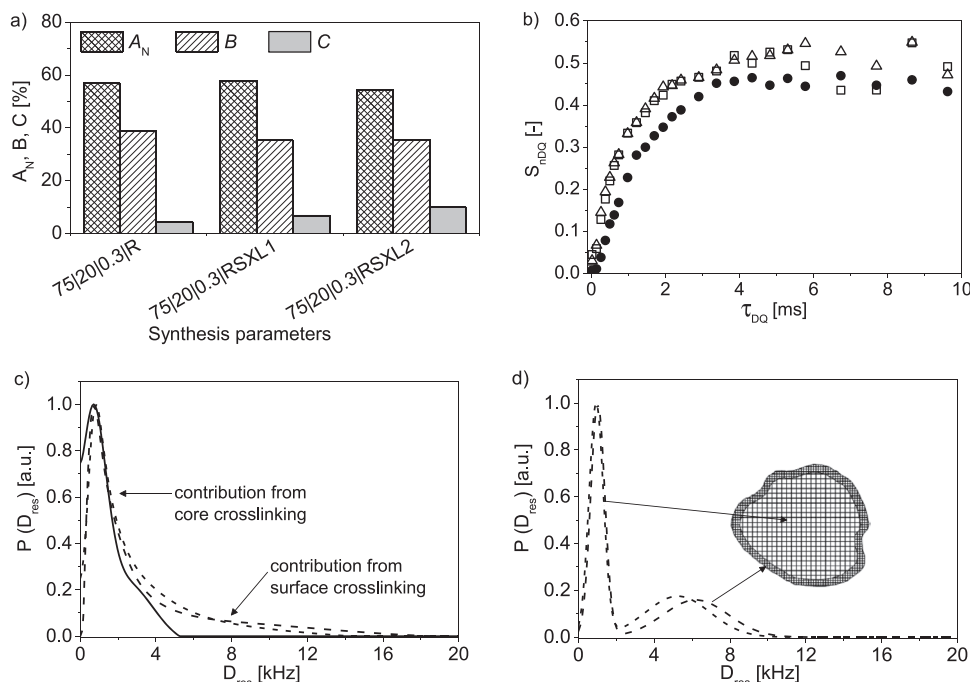


**Figure 5.** DQ-NMR results for samples SAP75|20|0.3|R without and with surface crosslinking (SXL). a) Fractions of network chains  $A_N$ , mobile components  $C$ , and network defects  $B$ . b) Normalized DQ build-up signals ( $\bullet$ ,  $R$ ;  $\square$ , RSXL1;  $\triangle$ , RSXL2). c) Corresponding RDC distributions retrieved by regularization ( $-$ ,  $R$ ;  $- \cdot -$ , SXL1; and  $- - -$ , SXL2), d) RDC distributions for “core-shell” crosslinked hydrogel particles ( $- \cdot -$ , SXL1;  $- - -$ , SXL2) obtained with a bimodal Gaussian distribution.

regularization with two different kernel functions is small. For the sample SAP100|25|1, the relative distribution width obtained by regularization is larger than that by Gaussian fit. Such deviations can be attributed to the spatially inhomogeneous network structures from swelling if not to numerical instabilities. The inhomogeneity and/or heterogeneity in polymer gels is a nonideality affecting directly the physical properties of the gels such as swelling and turbidity.<sup>[55,56]</sup> Compared to other samples, the swollen sample SAP100|25|1 is more turbid, which indicates larger swelling inhomogeneity because the turbidity of a gel is a direct result of light scattered from the inhomogeneity of its refractive index. The occurrence of swelling inhomogeneity also makes the RDC distribution obtained using the Gaussian model fit deviate from the real distribution in this case, leading to a broad RDC distribution and thus to a large relative distribution width in the regularization procedure. A similar phenomenon has been observed in a swollen sample SAP75|20|0.3|RSXL2, behaving like a “core-shell” particle with different core and surface crosslinking densities.<sup>[45]</sup> The RDC distribution reflects contributions from both core and surface crosslinking. In this case, when a monomodal Gaussian-distributed fitting function, Equation (2), is used to model the DQ build-up signals (Figure 5b) from such “core-shell” crosslinked hydrogels, the resulting RDC distribution will become broader. However, the results obtained with a bimodal distribution or numerical regularization have a clearly defined physical meaning (Figure 5c,d). Summarizing, a good correlation and agreement between the results obtained with different methods has been found within the experimental reliability (Figure 6).

### 3.3.4. Impact of Temperature, Swelling, and Solvent of SAP in DQ-NMR

Different SAP hydrogels were investigated by low-field <sup>1</sup>H DQ-NMR due to the instrument robustness, low cost, and ease of handling. Some influencing factors such as sample preparation, swelling solvent, swelling degree, and duration as well as sample temperature are considered and discussed.

As stated above, dry gel powders were washed with 99.9% deuterated D<sub>2</sub>O to reduce volatile substances. The fraction of mobile sol components for the sample without washing is about 10.8% (Figure 7a), which is twice as high as that for the sample after washing. The difference between two corresponding  $S_{n,DQ}$  curves is not significant at  $\tau_{DQ} < 15$  ms although the data scatter at  $\tau_{DQ} > 15$  ms (Figure 7b). RDC distributions for samples with and without washing are given by  $D_{res,mean} = 3.2$  kHz,  $\sigma = 1.9$  kHz and  $D_{res,mean} = 3.6$  kHz,  $\sigma = 2.0$  kHz, respectively. The relative deviations of  $D_{res,mean}$  and of  $A_N$  are both in the range of 12%. Experiments on samples after washing twice indicate that the fraction of mobile components decreased, but the impact on  $D_{res,mean}$  and  $A_N$  is small with relative deviations of less than 10%. To avoid time-consuming sample preparation, one washing was performed for all samples in this work.

The same solvent (99.9% deuterated D<sub>2</sub>O) was used during swelling to reduce solvent protons. When the sample is swollen in H<sub>2</sub>O, the detected relative DQ signal intensity becomes

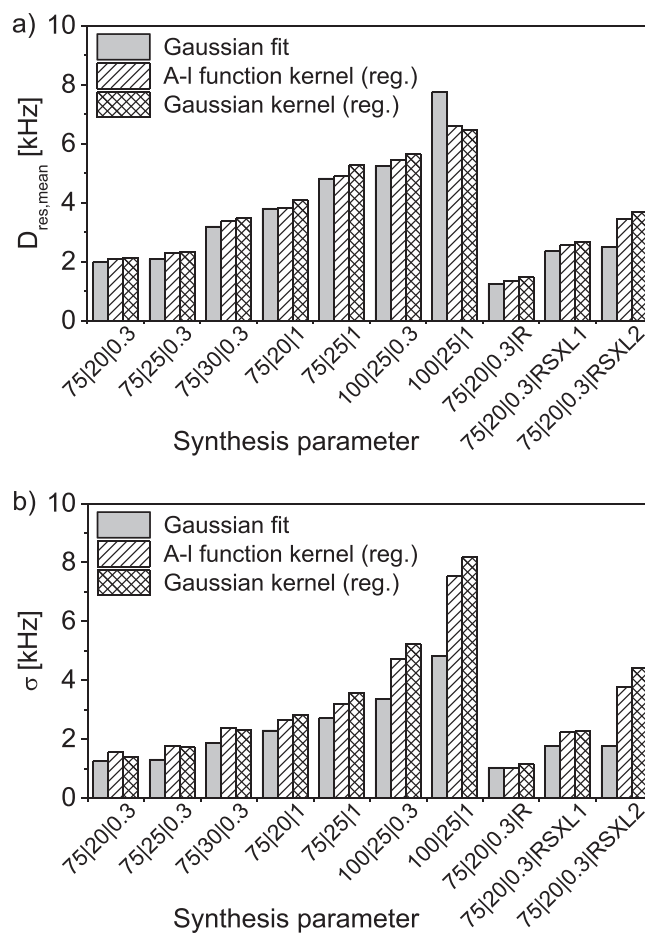


**Figure 6.** RDC distributions obtained by Gaussian-distributed fitting function according to Equation (2), and by regularization with Gaussian and A-I function kernels [Equations (3)–(5)]. a) Mean RDC  $D_{res,mean}$ . b) Distribution width  $\sigma$ .

weak and noisy. For example, the DQ signal from the sample swollen in D<sub>2</sub>O reaches more than 20% (cf. Figure 1), while the DQ signal from the same sample swollen in H<sub>2</sub>O is lower than 1%. Chemical exchange occurs between <sup>1</sup>H of swelling solvent and the exchangeable <sup>1</sup>H of the polymer chains. DQ coherences arise from the almost nonexchangeable protons of the polymer, since the DQ signal is dominated by spin-pair DQ coherences.<sup>[38,49]</sup> The utilization of nondeuterated or partially deuterated solvent as swelling solvent will make it difficult or sometimes even impossible to detect DQ signals in low-field <sup>1</sup>H DQ-NMR experiments with a good S/N value.

Furthermore, <sup>1</sup>H DQ-NMR experiments performed at different sample temperatures (39.5 and 55 °C) show that higher temperature reduces the measured fraction of network defects, but the measured fraction of mobile components increases (Figure 8a). The assignment might be questionable. Nevertheless, at a high temperature, the mobile components tend to move faster, and the defect components will partially become mobilized. The measured fraction of uncoupled network defects may significantly depend on the crosslink density and in particular on the temperature.<sup>[36,50]</sup> However, the couplings are closely related to the local

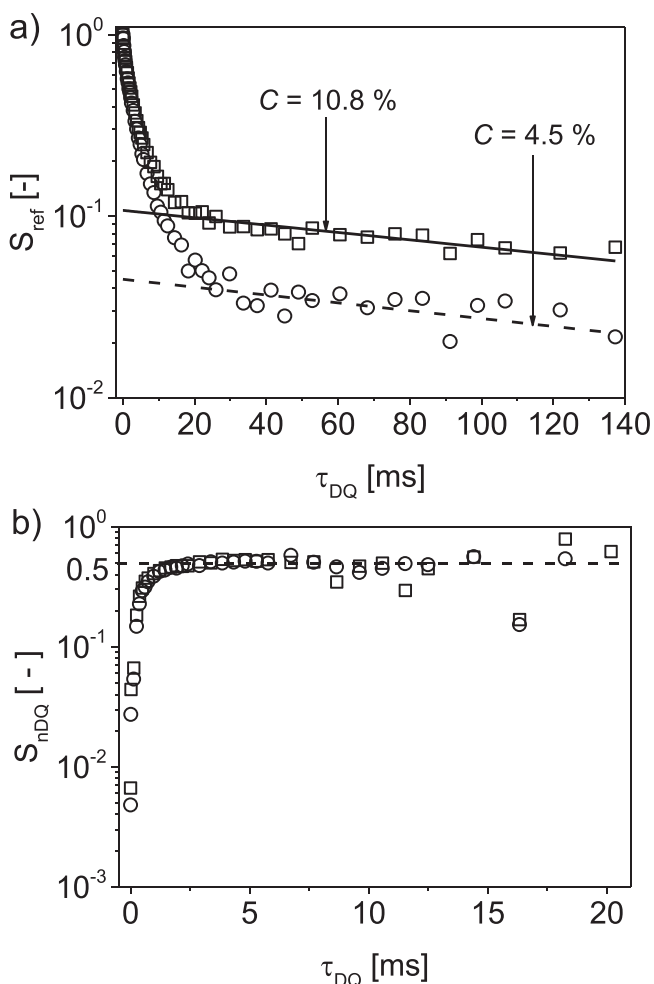


**Figure 7.** a)  $S_{ref}$  and b)  $S_{nDQ}$  of SAP75[30]0.3 with prewashing (experimental data:  $\circ$ , and fitting curve: dashed line) and without prewashing (experimental data:  $\square$ , and fitting curve: solid line).

crosslinking density and the chain length between restrictions. The normalized DQ build-up signals show very small difference (Figure 8b). Such a behavior was observed in previous DQ-NMR studies.<sup>[32,49]</sup> As expected, the fraction of network chains is only slightly influenced by temperature. The relative deviations of  $D_{res,mean}$  and of  $A_N$  are both less than 10% for the investigated temperatures. This is also the case for different crosslinking levels (DC = 0.3 and 1 mol%) at the same monomer concentration. Besides the physical entanglements in hydrogels, such differences may also be attributed to the measurement error.

DQ experiments on the hydrogels for different swelling durations (1 day and 8 weeks) exhibit similar behavior, i.e., small differences for both RDC and  $A_N$ . However, the  $C$  fraction increased with swelling duration. For hydrogels with DN = 75 mol%, the increase in  $C$  is more pronounced than that with DN = 100 mol%. An explanation could be that small polymer chains diffuse out and become more mobile. This is called constraint release. The two  $-COOH$  hydrogen bridges in SAP hydrogels have a bond energy of about  $30 \text{ kJ mol}^{-1}$  and thus the constraint release will take time as every chain has several of those.

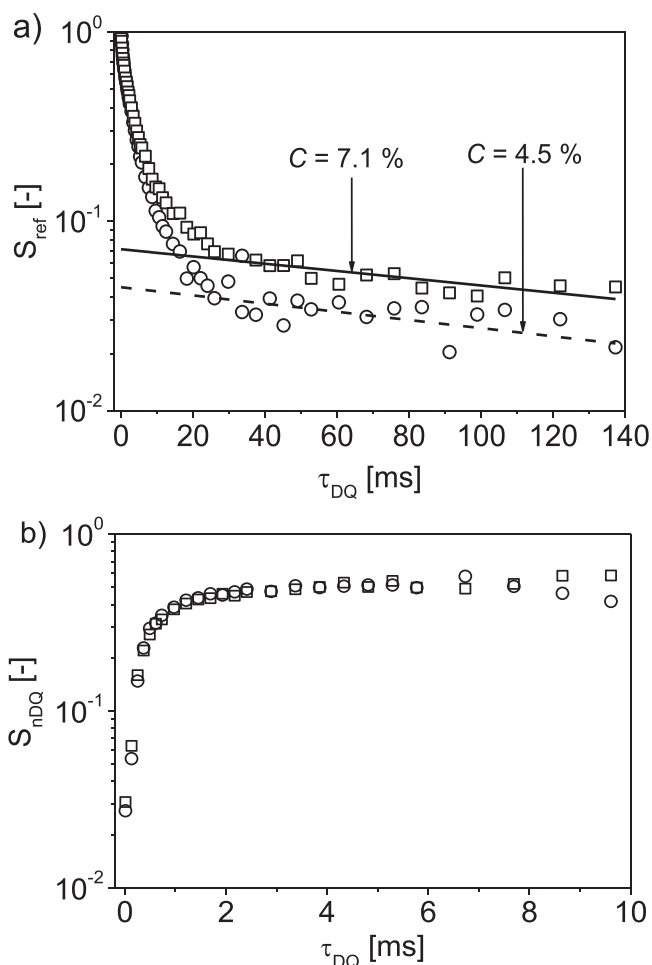


**Figure 8.** DQ-NMR signal for SAP75[30]0.3 obtained at temperatures of  $39.5 \text{ }^\circ\text{C}$  (experimental data:  $\circ$ , and fitting curve: dashed line) and  $55 \text{ }^\circ\text{C}$  (experimental data:  $\square$ , and fitting curve: solid line). a) Reference decay signals. b) Normalized DQ build-up signals.

DQ experiments on identical hydrogels swollen at a mass ratio of 1:5 indicate that the evolution time becomes longer to reach the plateau value of 0.5 for  $S_{nDQ}$  (Figure 9), as compared to the observations for a swelling ratio of 1:9. The RDC distribution has a smaller mean RDC value and a narrower width. It is also found that the ratio of  $D_{res,mean}$  is close to the ratio of their swelling degrees. As RDCs rely on the fluctuating dipolar coupling tensor with respect to the magnetic field, they are proportional to the local dynamic order parameter of the polymer backbone. Fast segmental dynamics of the polymer chains leads to a loss of correlation to a plateau value related to the existence of preferential local orientation generated from crosslinking.<sup>[32,57]</sup> At a lower swelling degree, polymer chains in a gel are less stretched and therefore become more mobile. The  $T_2$ -relaxation time of the polymer networks increases because the correlation time of the polymer chains decreases, leading to a smaller  $D_{res,mean}$ . The relative distribution width  $r = \sigma/D_{res,mean}$  remains nearly constant for the same hydrogel at both swelling degrees. The detected fraction of network chains is somewhat larger at the lower swelling degree, which can be attributed to a smaller contribution from fractions of network

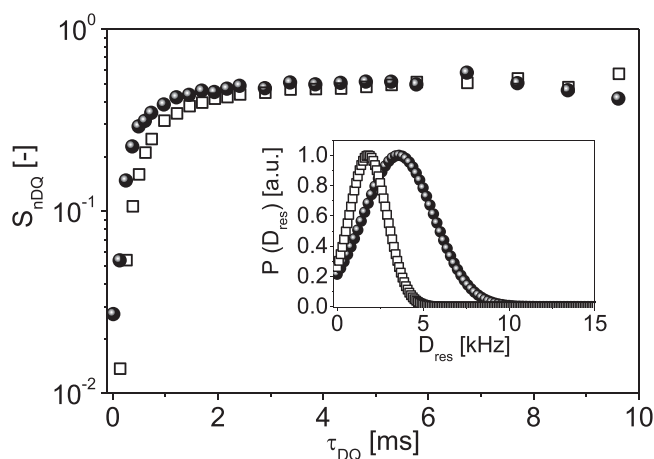


**Figure 9.** DQ build-up curves for SAP75[30]0.3 measured at different swelling degrees, SAP:D<sub>2</sub>O = 1:9 (●) and 1:5 (□). The inset shows the corresponding RDC distributions.

defects and mobile sol components. Similar behavior has been observed in other SAP hydrogels with different crosslink densities in the current work.

#### 4. Conclusions

SAP hydrogels have been investigated by <sup>1</sup>H DQ-NMR. A fit model was developed to reliably extract structural parameters from DQ-NMR experiments. As compared to the common fit, this approach is user independent. <sup>1</sup>H DQ-NMR provided the RDC distribution ( $D_{res,mean}$ ,  $\sigma$ ), the fractions of network defects, and mobile sol components as well as network chains. DQ-NMR revealed the correlation between the complex topology of the hydrogels and synthesis parameters. With increasing crosslinking, both RDCs and the fraction of network chains increased, but the fraction of network defects decreased. The same characteristics have also been observed when increasing the solid content in the synthesis of SAP. With increasing degree of neutralization, both RDCs and the fraction of network defects increased, but the fraction of network chains decreased. Some influencing factors in the <sup>1</sup>H DQ-NMR such as sample preparation, swelling solvent, swelling degree and duration, measuring temperature, and recycle delay have also been studied. The results led to a better understanding of the topology, local mobility, and respective heterogeneity of SAP and their correlation with synthesis parameters.

The knowledge of a <sup>23</sup>Na and <sup>1</sup>H translational dynamics will help to predict the mobility of molecules and ions within the polymer networks, which will be investigated in future work. <sup>23</sup>Na-relaxation and <sup>23</sup>Na- and <sup>1</sup>H pulsed field-gradient NMR diffusion will allow for a more comprehensive description of the translational dynamics of <sup>23</sup>Na<sup>+</sup> and water molecules in the swollen gel.

#### Acknowledgements

Prof. K. Saalwächter kindly provided the low-field DQ pulse sequence. Financial support from the German Research Foundation (DFG) is

highly appreciated (DFG SFB 1176 Project Q2 as well as Pro<sup>2</sup> NMR instrumental facility at KIT and RWTH Aachen).

#### Conflict of Interest

The authors declare no conflict of interest.

#### Keywords

<sup>1</sup>H double-quantum NMR, hydrogels, network defects, residual dipolar coupling, superabsorbent polymers

Received: March 15, 2018

Revised: April 12, 2018

Published online: May 25, 2018

- [1] M. J. Zohuriaan-Mehr, H. Omidian, S. Doroudiani, K. Kabiri, *J. Mater. Sci.* **2010**, *45*, 5711.
- [2] R. Dhodapkar, N. N. Rao, S. P. Pande, T. Nandy, S. Devotta, *React. Funct. Polym.* **2007**, *67*, 540.
- [3] J. El-Asmar, H. Jaafar, I. Bashour, M. T. Farran, I. P. Saoud, *Clean: Soil, Air, Water* **2017**, *45*, 1700251.
- [4] M. R. Guilherme, F. A. Aouada, A. R. Fajardo, A. F. Martins, A. T. Paulino, M. F. T. Davi, A. F. Rubira, E. C. Muniz, *Eur. Polym. J.* **2015**, *72*, 365.
- [5] M. E. Parente, A. Ochoa Andrade, G. Ares, F. Russo, Á. Jiménez-Kairuz, *Int. J. Cosmet. Sci.* **2015**, *37*, 511.
- [6] C. Merle, G. Kummerlöwe, J. C. Freudenberger, F. Halbach, W. Stöwer, C. L. v. Gostomski, J. Höpfner, T. Beskers, M. Wilhelm, B. Luy, *Angew. Chem., Int. Ed.* **2013**, *52*, 10309.
- [7] M. F. Akhtar, M. Hanif, N. M. Ranjha, *Saudi Pharm. J.* **2016**, *24*, 554.
- [8] J. Maitra, V. K. Shukla, *Am. J. Polym. Sci.* **2014**, *4*, 25.
- [9] M. J. Zohuriaan-Mehr, K. Kabiri, *Iran. Polym. J.* **2008**, *17*, 451.
- [10] F. L. Buchholz, A. T. Graham, *Modern Superabsorbent Polymer Technology*, Wiley-VCH, New York, NY **1998**.
- [11] F. Di Lorenzo, S. Seiffert, *Polym. Chem.* **2015**, *6*, 5515.
- [12] O. Okay, in *Hydrogel Sensors and Actuators: Engineering and Technology* (Eds: G. Gerlach, K.-F. Arndt), Springer, Berlin **2010**, p. 1.
- [13] M. Shibayama, *Macromol. Chem. Phys.* **1998**, *199*, 1.
- [14] M. Y. Kizilay, O. Okay, *Macromolecules* **2003**, *36*, 6856.
- [15] N. Orakdogan, O. Okay, *Polym. Bull.* **2006**, *57*, 631.
- [16] S.-i. Takata, T. Norisuye, M. Shibayama, *Macromolecules* **1999**, *32*, 3989.
- [17] W. Chasse, S. Schlogl, G. Riess, K. Saalwächter, *Soft Matter* **2013**, *9*, 6943.
- [18] H. Aoki, S. Tanaka, S. Ito, M. Yamamoto, *Macromolecules* **2000**, *33*, 9650.
- [19] F. B. Madsen, A. E. Daugaard, C. Fleury, S. Hvilsted, A. L. Skov, *RSC Adv.* **2014**, *4*, 6939.
- [20] G. M. Conley, S. Nöjd, M. Braibanti, P. Schurtenberger, F. Scheffold, *Colloids Surf., A* **2016**, *499*, 18.
- [21] A. Izumi, T. Nakao, H. Iwase, M. Shibayama, *Soft Matter* **2012**, *8*, 8438.
- [22] G. Patras, G. G. Qiao, D. H. Solomon, *Macromolecules* **2001**, *34*, 6396.
- [23] J. Habel, A. Ogbonna, N. Larsen, S. Cherre, S. Kynde, S. R. Midtgaard, K. Kinoshita, S. Krabbe, G. V. Jensen, J. S. Hansen, K. Almdal, C. Helix-Nielsen, *RSC Adv.* **2015**, *5*, 79924.
- [24] B. Lindemann, U. P. Schröder, W. Oppermann, *Macromolecules* **1997**, *30*, 4073.



- [25] I. Yazici, O. Okay, *Polymer* **2005**, *46*, 2595.
- [26] G. R. Deen, T. Alsted, W. Richtering, J. S. Pedersen, *Phys. Chem. Chem. Phys.* **2011**, *13*, 3108.
- [27] M. Shibayama, *Polym. J.* **2011**, *43*, 18.
- [28] M. Shibayama, T. Tanaka, C. C. Han, *J. Chem. Phys.* **1992**, *97*, 6829.
- [29] B. Strachota, L. Matejka, A. Zhigunov, R. Konefal, J. Spevacek, J. Dybal, R. Puffr, *Soft Matter* **2015**, *11*, 9291.
- [30] A. M. Amorim da Costa, A. M. Amado, *Solid State Ionics* **2001**, *145*, 79.
- [31] K. Saalwächter, W. Chasse, J. U. Sommer, *Soft Matter* **2013**, *9*, 6587.
- [32] K. Saalwächter, *Prog. Nucl. Magn. Reson. Spectrosc.* **2007**, *51*, 1.
- [33] W. Chasse, J. L. Valentin, G. D. Genesky, C. Cohen, K. Saalwächter, *J. Chem. Phys.* **2011**, *134*, 044907.
- [34] J. Höpfner, G. Guthausen, K. Saalwächter, M. Wilhelm, *Macromolecules* **2014**, *47*, 4251.
- [35] K. Saalwächter, in *Modern Magnetic Resonance* (Ed: G. A. Webb), Springer International Publishing, Cham, Switzerland **2017**, p. 1.
- [36] W. Chasse, M. Lang, J. U. Sommer, K. Saalwächter, *Macromolecules* **2012**, *45*, 899.
- [37] H. Li, *Smart Hydrogel Modelling*, Springer, Berlin **2009**.
- [38] R. Graf, A. Heuer, H. W. Spiess, *Phys. Rev. Lett.* **1998**, *80*, 5738.
- [39] K. Saalwächter, *ChemPhysChem* **2013**, *14*, 15.
- [40] I. Schnell, H. W. Spiess, *J. Magn. Reson.* **2001**, *151*, 153.
- [41] B. Wu, W. Chassé, R. Peters, T. Brooijmans, A. A. Dias, A. Heise, C. J. Duxbury, A. P. M. Kentgens, D. F. Brougham, V. M. Litvinov, *Macromolecules* **2016**, *49*, 6531.
- [42] L. Masaro, X. X. Zhu, *Prog. Polym. Sci.* **1999**, *24*, 731.
- [43] A. H. Muhr, J. M. V. Blanshard, *Polymer* **1982**, *23*, 1012.
- [44] Y. A. Hussain, T. Liu, G. W. Roberts, *Ind. Eng. Chem. Res.* **2012**, *51*, 11401.
- [45] M. Elliott, *Superabsorbent Polymers*, BASF-Ag. **2004**.
- [46] K. Saalwächter, M. Gottlieb, R. G. Liu, W. Oppermann, *Macromolecules* **2007**, *40*, 1555.
- [47] J. Weese, *Comput. Phys. Commun.* **1993**, *77*, 429.
- [48] J. Weese, *Comput. Phys. Commun.* **1992**, *69*, 99.
- [49] K. Saalwächter, P. Ziegler, O. Spyckerelle, B. Haidar, A. Vidal, J. U. Sommer, *J. Chem. Phys.* **2003**, *119*, 3468.
- [50] J. L. Valentin, P. Posadas, A. Fernandez-Torres, M. A. Malmierca, L. Gonzalez, W. Chasse, K. Saalwächter, *Macromolecules* **2010**, *43*, 4210.
- [51] B. Gabrielle, E. Gomez, J. P. Korb, *J. Phys. Chem. B* **2016**, *120*, 5581.
- [52] A. Naumova, C. Tschierske, K. Saalwächter, *Solid State Nucl. Magn. Reson.* **2017**, *82*, 22.
- [53] N. Tsukida, H. Muranaka, M. Ide, Y. Maeda, H. Kitano, *J. Phys. Chem. B* **1997**, *101*, 6676.
- [54] N. Moini, K. Kabiri, M. J. Zohuriaan-Mehr, *Polym.-Plast. Technol. Eng.* **2016**, *55*, 278.
- [55] S. Kara, O. Okay, Ö. Pekcan, *Polym. Bull.* **2000**, *45*, 281.
- [56] O. Okay, Y. Yilmaz, D. Kaya, M. Keskinel, Ö. Pekcan, *Polym. Bull.* **1999**, *43*, 425.
- [57] J. L. Valentin, D. López, R. Hernández, C. Mijangos, K. Saalwächter, *Macromolecules* **2009**, *42*, 263.